DE GRUYTER OPEN

Influence of preparation method on structural, optical and magnetic properties of nickel ferrite nanoparticles

AYAZ ARIF KHAN[1],[*], M. JAVED[1], A. RAUF KHAN[1], YOUSAF IQBAL[1], ASIF MAJEED[1], SYED ZAHID HUSSAIN[2], S.K. DURRANI[2]

[1]Department of Physics, University of Azad Jammu & Kashmir, 13100 Muzaffarabad, Pakistan

[2]Materials Division, Directorate of Technology, Pakistan Institute of Nuclear Science and Technology, P.O. Nilore, Islamabad 45650, Pakistan

Nanocrystalline $NiFe_2O_4$ particles were prepared by conventional sol-gel, citrate-nitrate sol-gel combustion and co-precipitation methods. The synthesized samples were annealed at 1000 °C for two hours and structural, chemical, morphological, optical and magnetic properties of nickel ferrite were investigated. The structural properties were investigated by X-ray diffraction (XRD) technique which confirmed the formation of single phase $NiFe_2O_4$ particles derived by the three methods. The chemical properties were analyzed by Fourier transform infrared (FT-IR) spectroscopy which confirmed the corresponding vibration modes in the samples. The optical properties were studied by UV-Vis spectroscopy. The morphological study of the as-synthesized samples was carried out by scanning electron microscopy (SEM). SEM images showed the agglomerated nanoparticles of $NiFe_2O_4$. The magnetic properties were investigated by vibrating sample magnetometer (VSM), which showed that the calcined samples exhibited typical magnetic behavior.

Keywords: *NFO magnetic properties; NFO structural properties; NFO morphology*

© Wroclaw University of Science and Technology.

1. Introduction

Ferrites constitute the most important class of soft magnetic materials due to their influential properties which comprise high specific heat, low melting point, large coefficient of expansion, low temperature of magnetic phase transition and magnetic moments with low saturation [1, 2]. These interesting properties make them attractive candidates in practical applications, such as gas sensors [3], microwave and electronic devices [4], telecommunication equipment [5], magnetic storage [6] and magnetic fluids [7]. In addition, ferrites are also used for biomedical purposes, such as inter-body drug delivery [8, 9] and hypothermia [10]. The nanosized ferrites have spinel structure with structural formula MFe_2O_4, where M can be a divalent metal ion such as Ni, Cu, Zn, Co, Mn, Mg, etc. [11]. The noteworthy magnetic and electrical characteristics of ferrite nanocrystals are based

on the nature of ions and the type of charge in them as well as the distribution of these ions on tetrahedral (A) and octahedral (B) sites. Among numerous ferrites, nickel ferrite is a versatile and technologically prominent soft magnetic ceramic material due to its very attractive properties, such as high electrical resistivity, high electrochemical stability [12], high Curie temperature [13], low magnetostriction [14], low magnetic coercively, low magnetic anisotropy [15], high permeability in RF region [16], high Neel temperature [17], etc. In addition, nickel ferrite has low eddy current loss which makes it a desired core material for the power transformers [18].

The crystal structure of nickel ferrite is inverse spinel. This structure is face centered cubic, having 32 oxygen ions in the unit cell. These oxygen ions occupy 64 tetrahedral and 32 octahedral sites. That is, in nickel ferrite, ferric ions (Fe^{3+}) occupy A sites whereas B sites are taken by 1:1 mixture of the nickel ions (Ni^{2+}) and ferric ions (Fe^{3+}). Ni^{2+} ions are situated at B sites

---

and are coordinated octahedrally by the surrounding O^{2-} ions. Thus, the compound can be expressed by the formula $(Fe^{3+})_A[Ni^{2+}Fe^{3+}]_BO_4^{2-}$ [19, 20]. The ferromagnetic behavior of this ferrite is due to the magnetic moments with anti-parallel spins arising between Fe^{+3} ions situated at tetrahedral positions and Fe^{+3} and Ni^{+2} ions at octahedral positions [21]. The characteristic behaviors of $NiFe_2O_4$ are connected with the structure and microstructural building blocks of the nanoparticles which are very sensitive to the applied synthesis routes. The ferrite nanoparticles have been developed by several chemical and physical techniques which include sonochemical reactions [22], solid state reactions [23], microwave plasma [24], high temperature self-propagation [25], solvothermal synthesis [26], sol-gel methods [27], chemical co-precipitation [28], hydrothermal method [29], etc. Besides, sol-gel wet chemical, sol-gel auto-combustion and co-precipitation methods are very favorable [30–32]. Conventional sol-gel method is useful due to its various advantages, such as possibility to achieve a very small particle size, high homogeneity, easy shaping and doping, good stoichiometric control and better phase purity in comparison with the conventional ceramic methods [18, 33]. The sol-gel auto-combustion method is useful due to the advantages of cheap precursors, simple synthesis, yielding an ultrafine and homogeneous powder [34]. In contrast, co-precipitation method is used in consequence of its advantages which are low temperature, easy control of average grain size by controlling the precipitation reaction and high production rate [32]. In this study, $NiFe_2O_4$ nanoparticles were synthesized by conventional sol-gel (CSG), citrate-nitrate sol-gel combustion (SGC) and co-precipitation (Co-P) routes. The microstructures as well as the magnetic properties of the sintered CSG, SGC and Co-P derived samples were investigated and a critical comparison is presented.

2. Experimental

The schematic flowchart of different experimental procedures used for the preparation of $NiFe_2O_4$ nanopowders is illustrated in Fig. 1. The starting materials in all three routes were iron nitrate $[(Fe(NO_3)_3\cdot9H_2O)]$ and nickel nitrate $[(Ni(NO_3)_2\cdot6H_2O)]$. All the reagents of analytical grade with a high purity of 99.99 % were used as received without further purification.
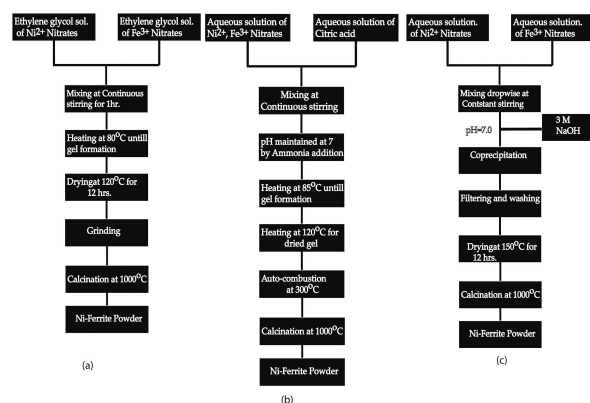

Fig. 1. Scheme of synthesis of $NiFe_2O_4$ powders by (a) CSG route, (b) SGC route and (c) the Co-P route.

In CSG route, metal salts were separately dissolved in ethylene glycol under magnetic stirring. These two solutions were then mixed together and kept under constant stirring for one hour. The clear solution obtained after stirring was heated in an electric oven at 80 °C to get a wet gel. The gel was dried at 120 °C in the same oven for 12 hours. Self-ignition took place yielding a fluffy and highly voluminous product with brown color. The powder obtained in this way was ground and annealed at 1000 °C for two hours in an electric furnace.

In SGC, citric acid monohydrate was used both as chelating agent and fuel for the combustion process. Deionized water was used to dissolve all the starting metal salts, with molar ratios of citrate/nitrate (C/N) equal to 1. The pH value of the solution was adjusted to about 7 by adding small amount of ammonia. During this process, the solution remained under continuous stirring by using a magnetic bar agitator. The resulting solution was heated under stirring at 85 °C to evaporate the excess of solvent and to form a gel. The gel was transferred into a bowl and was heated on a hot plate at 120 °C. At temperature of 300 °C,

the dried gel started burning in a self-propagating auto-combustion manner until the whole gel was completely burnt out to yield a loose powder. This powder was finally annealed at 1000 °C for two hours to obtain the final product.

For Co-P route the stoichiometric amount of metal salt was dissolved separately in an appropriate amount of deionized water. The prepared solutions were mixed by using a micropipette under continuous stirring. The pH value of the solution was accurately maintained by dropping sodium hydroxide (NaOH) solution, where this sodium hydroxide solution acted as precipitating agent. In this way, the precipitates with brown color were formed. Sodium hydroxide as well as other impurities were removed by filtering and washing the precipitates many times with deionized water. The precipitate was dried for two hours at 150 °C in the electric oven. The resulting product was milled and finally annealed for two hours at 1000 °C to get the final fine nickel ferrite ($NiFe_2O_4$) nanoparticles.

3. Characterization

The structural investigation of the annealed powders of the samples was performed by using X-ray diffractometer (Rigaku DMAX-3A) with CuKα radiation (1.5406 Å). For examining microstructure of all the calcined samples, the scanned micrographs were taken by JEOL JSM-6510LV scanning electron microscope (SEM) machine. The Fourier transform infrared spectra were taken by Perkin-Elmer 100 Series FT-IR spectrometer with potassium bromide (KBr) as a solvent. The optical characterization was performed by using Perkin-Elmer, LAMBDA 950 UV-Vis-NIR spectrometer. The magnetic properties were probed by magnetic hysteresis loops of the final powders characterized by vibrating sample magnetometer (VSM).

4. Results and discussion

Fig. 2 shows the XRD patterns of $NiFe_2O_4$ powder specimens synthesized by CGS, SGC and Co-P methods. The sharp peaks appearing

in the diffractograms show fully crystalline phase of nickel ferrite ($NiFe_2O_4$) with well pronounced cubic spinel crystal structure. The main peak is centered at $2\theta = 35.7°$ and corresponds to the crystal plane with Miller indices (3 1 1) which is characteristic of $NiFe_2O_4$ cubic spinel. The sharp peaks in XRD patterns are according to standard JCPDS Card No. 74-2081. After indexing the peak positions and relative intensities of the XRD pattern (Fig. 2), it was revealed that the synthesized powder samples calcined at 1000 °C is cubic spinel nickel ferrite ($NiFe_2O_4$) with space group Fd3m. However, few impurity peaks were observed in auto-combustion derived sample which can be indexed according to standard JCPDS Card No. 87-1166 corresponding to the presence of hematite phase (α-Fe_2O_3).
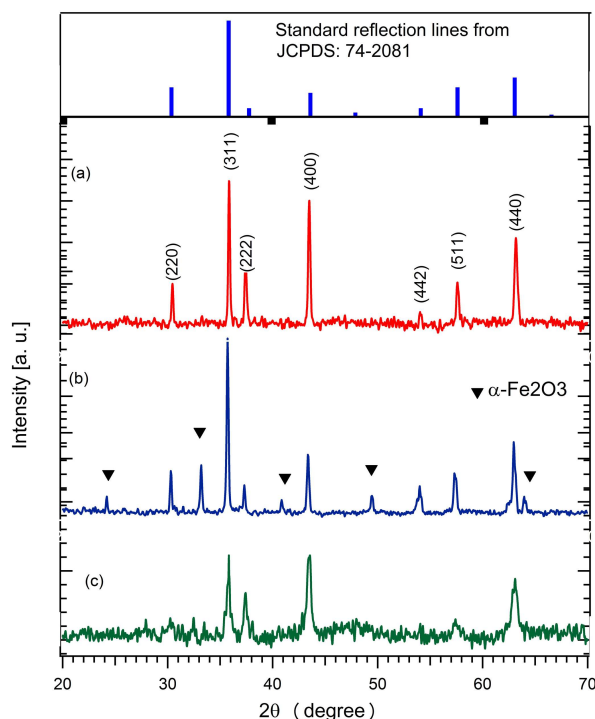

Fig. 2. XRD patterns of $NiFe_2O_4$ nanoparticles synthesized by (a) CSG, (b) SGC and (c) Co-P methods.

The average crystallite sizes of particles were calculated for all the samples using high intensity peak (3 1 1) with the help of the Debye-Scherrer equation [35]:

$$D = \frac{k\lambda}{\beta\cos\theta} \qquad (1)$$

where D is the average particle size, k is the particle shape factor (0.89), λ is the wavelength of the X-ray beam used (0.154 nm), β is the full width at half- maximum (FWHM) of (3 1 1) plane and θ is Bragg's angle. The calculated values of the average crystallite sizes are listed in the Table 1. The average lattice constant a for (3 1 1) plane was determined using the equation:

$$a = \frac{\sqrt{h^2 + k^2 + l^2}}{2\sin\theta} \qquad (2)$$

and is listed in Table 1 for all samples. The obtained values are in good agreement with the literature [36].

The average X-ray density of the nickel ferrite nanoparticles was determined using the relation:

$$\rho_x = 8M/Na^3 \qquad (3)$$

where M is the molecular weight (for nickel ferrite: 234.3816 g·mol^{-1}), N is Avogadro's number (6.02×10^{23} mol^{-1}) and a is lattice constant.

Fig. 3 shows FT-IR spectra of investigated $NiFe_2O_4$ samples which helps to confirm the synthesis of spinel structure. In infrared region, two main frequency modes are observed within the wave number range of 1000 cm^{-1} to 300 cm^{-1}. The higher band (ν_1), generally observed in the range of 600 cm^{-1} to 550 cm^{-1}, is attributed to the stretching frequency of tetrahedral metal-oxygen bond and the lowest band (ν_2), commonly observed in the range 450 cm^{-1} to 385 cm^{-1}, is assigned to vibration mode of octahedral metal-oxygen bond [37].

The vibrational modes of infrared bands of the samples synthesized by sol-gel, auto-combustion and co-precipitation routes are given in the Table 2. Their values are in the perfect agreement with the values reported in the literature [37, 38]. The spectra also show the renowned bands near 3450 cm^{-1} and 1560 cm^{-1} which are ascribed to H–O stretching and bending vibrational modes of free or absorbed water. The band near 1420 cm^{-1} is caused by anti-symmetric NO-stretching modes,
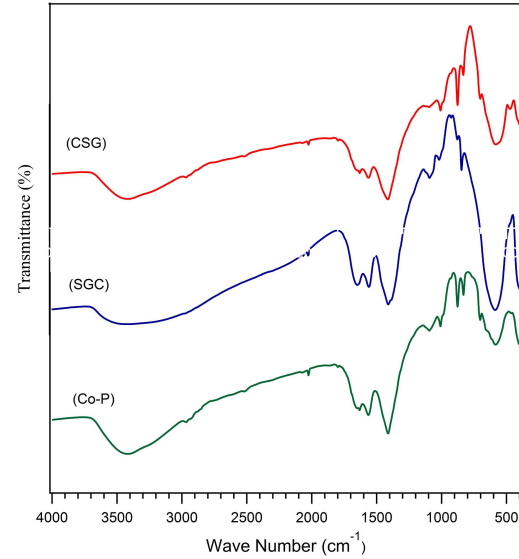

Fig. 3. FT-IR spectra of $NiFe_2O_4$ nanoparticles synthesized by CSG, SGC and Co-P methods.

which represents the residue nitrates in the samples [37].

Fig. 4 shows UV-Vis absorption spectra of sol-gel, auto-combustion and co-precipitation derived $NiFe_2O_4$ nanocrystals as a function of wavelength. The band gap energy was calculated using Tauc's plot. According to Tauc's equation [39, 40], for a direct bandgap material the absorption coefficient near the band edge is:

$$\alpha = \frac{A}{h\upsilon}\left(h\upsilon - E_g\right)^{\frac{1}{2}} \qquad (4)$$

where α is the absorption coefficient, $h\upsilon$ the photon energy, E_g the band gap energy, and A is a constant depending on the type of transition. Equation 4 can be rearranged and written in the form:

$$(\alpha h\upsilon)^2 = A^2\left(h\upsilon - E_g\right) \qquad (5)$$

From equation 5 it is clear that when $\alpha h\upsilon = 0$, then $E_g = h\upsilon$. The band gap energy is determined by plotting $(\alpha h\upsilon)^2$ against $h\upsilon$ and finding the intercept on the $h\upsilon$ axis by extrapolating the plot to $(\alpha h\upsilon)^2 = 0$. The band gap energy has been determined from the intercept of the straight line at $\alpha = 0$ for all samples and listed in Table 3. From Table 3 it can be seen that the band gap of the samples is in the range of 5.2 eV to 5.9 eV which is

Table 1. XRD analysis and magnetic characterization results of $NiFe_2O_4$ samples.

| Preparation technique	Annealing temperature [°C]	Crystallite size [nm]	X-ray density [g/cc]	Lattice constant [Å]
CSG	1000	70.73	5. 6049	8.2215
SGC	1000	26.71	4.8974	8.3253
Co-P	1000	35.35	5.3980	8.5998

Table 2. FT-IR frequency bands of $NiFe_2O_4$.

Synthesis route	IR frequency bands [cm^{-1}]	
	ν_1	ν_2
CSG	580	405
SGC	592	400
Co-P	586	401

comparable to the reported values [37]. The UV-Vis spectra of all samples clearly show that the $NiFe_2O_4$ nanocrystals can absorb energy in the wavelength range of 220 nm to 235 nm.

Table 3. Band gap and crystallite size of $NiFe_2O_4$.

Synthesis route	Band gap [eV]	Crystallite size [nm]
CSG	5.9	70.73
SGC	5.2	26.71
Co-P	5.8	35.35

The magnetic properties of $NiFe_2O_4$ nanoparticles were studied using VSM at room temperature. Fig. 5 shows the hysteresis loops of $NiFe_2O_4$ nanoparticles at an applied external magnetic field of ±15 kOe. The saturation magnetization (Ms), remanent magnetization (Mr) and coercivity (Hc) for CSG, SGC and Co-P derived samples are shown in Table 4. It is evident that the largest saturation magnetization of about 36.61 emu/g is observed for the CSG derived sample. The Ms values of the synthesized $NiFe_2O_4$ nanoparticles are significantly lower than those of the bulk $NiFe_2O_4$ (55 emu/g). The decrease in saturation magnetization of these samples, compared to that of bulk material, depends on different parameters. In the thermal treatment method, the heating rate of calcination process is one of the most important parameters that can effectively increase or decrease the saturation magnetization. In this investigation,
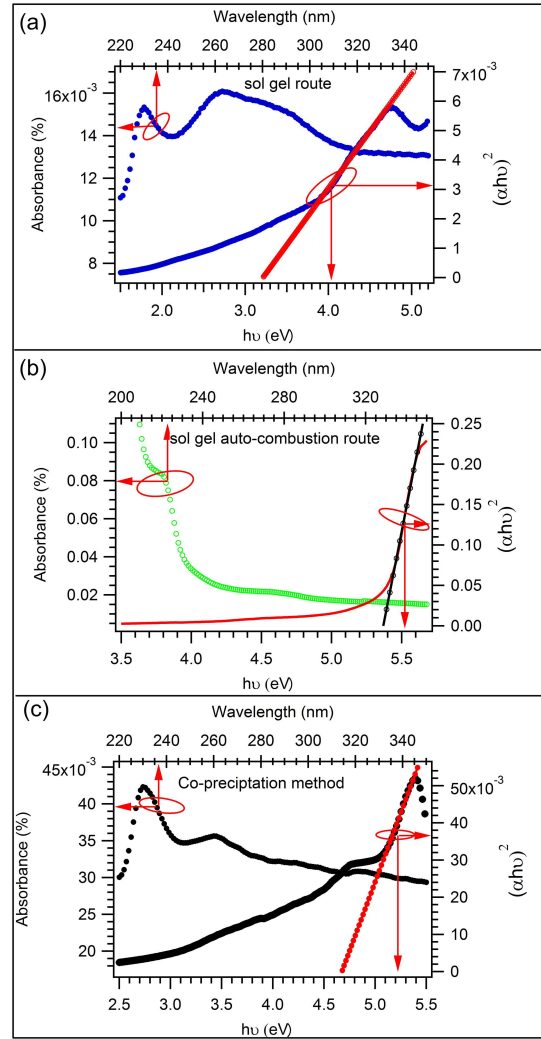
Fig. 4. UV-Vis spectra of $NiFe_2O_4$ nanoparticles synthesized by (a) CSG, (b) SGC and (c) Co-P methods.

the heating rate of calcination was about 10 °C/min which was a relatively high heating rate. Therefore, it is possible that calcination at a slower heating rate would allow the crystallization to be more
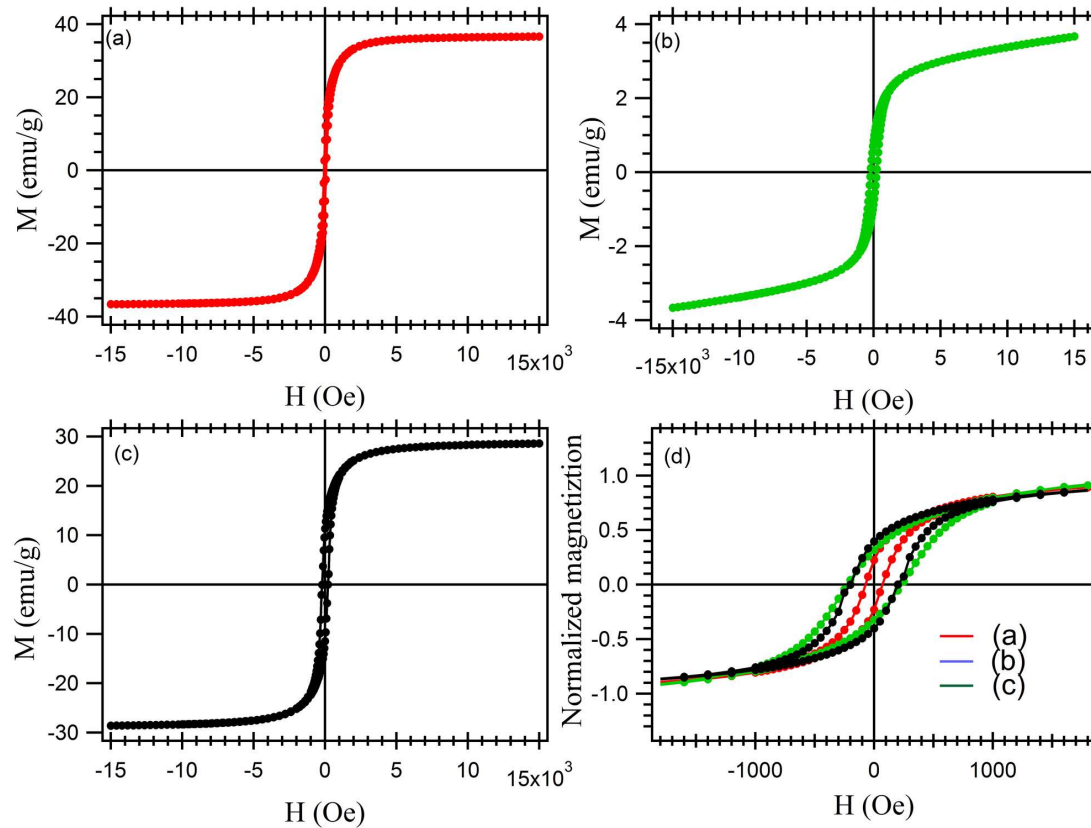
Fig. 5. Hysteresis curves of NiFe$_2$O$_4$ nanoparticles synthesized by (a) CSG, (b) SGC, (c) Co-P methods and (d) normalized M-H loops at ±1500 Oe.

Table 4. Average particle size [nm] of NiFe$_2$O$_4$ nanoparticles determined fromXRD and magnetic properties observed at room temperature by VSM.

Preparation technique	Crystallite size [nm]	Saturation magnetization M_S [emu/g]	Remanence M_R [emu/g]	Coercivity H_C [Oe]
CSG	70.73	36.61	8.252	72.3
SGC	26.71	3.6691	0.857	230
Co-P	35.35	28.58	11.341	201

complete, and the magnetic phase could also increase, resulting in larger saturation magnetization values [41].

However, a very low saturation magnetization of about 3.66 emu/g was observed in SGC derived sample which might be additionally caused by the appearance of the weakly magnetic, impure phase of hematite (Fig. 2). On the other hand, an increase in saturation magnetization was observed with increasing particle size. It may be due to the fact that the surface of the nanoparticles seems to possess slanted or distorted spins repelling the core spins in order to align the field direction. Subsequently, the saturation magnetization achieves smaller values [42–45]. Magnetic characterization reveals that the conventional sol-gel method produces nickel ferrite particles with moderate magnetization and very low hysteresis loss (Fig. 5d).

Scanning electron microscopy (SEM) was used to observe the influence of synthesis route on

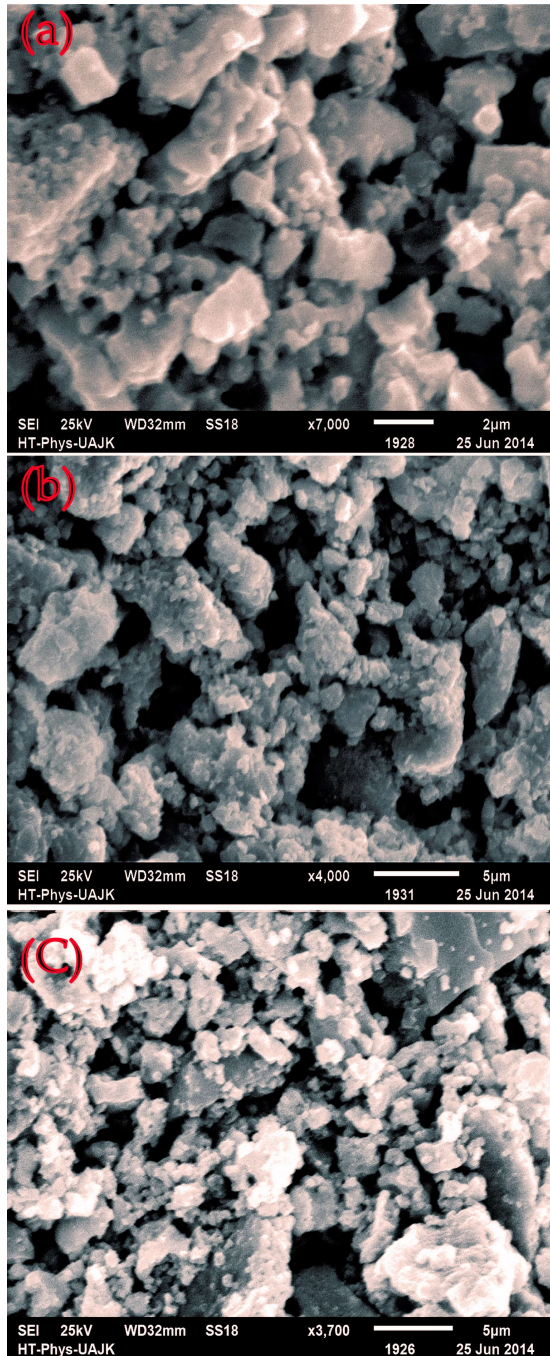morphology of the synthesized $NiFe_2O_4$ samples. Fig. 6 shows SEM images of $NiFe_2O_4$ powder calcined at 1000 °C.

Fig. 6. SEM images of $NiFe_2O_4$ nanoparticles synthesized by (a) sol-gel, (b) auto-combustion and (c) co-precipitation methods and calcined at 1000 °C.

The micrographs show highly crystallized particles which are agglomerated to form irregular structures. The formation of agglomerates could be due to the magnetic attraction. Still, there is a very large number of crystals with uniform size distribution. However, a large crystal size in the sol-gel derived sample compared to the other two is observed where grain size reached around 0.4 μm to 2.5 μm (Fig. 6a). These results are comparable with XRD data, where the sharp peaks are the indication of well-defined crystallization of $NiFe_2O_4$ which reveals that synthesis route has a significant effect on particle morphology and structure.

5. Conclusions

We have succeeded in synthesizing nickel ferrite nanoparticles by sol-gel wet chemical, sol-gel auto-combustion and co-precipitation methods. XRD results confirmed the crystallinity of particles. The sol-gel derived sample showed higher purity compared to the other two. The magnetic characterization clearly revealed that the sol-gel method produced nanoparticles with moderate magnetization and low hysteresis loss. The smaller value of M_S compared to the bulk value in the prepared samples was attributed to the greater fraction of surface spins in these nanoparticles that tended to be in a canted, spin-glass-like-ordered phase, like a state with a small magnetic moment. The high level of crystallinity, moderate magnetization and low hysteresis loss in the sol-gel derived sample makes sol-gel wet chemical method the best choice for synthesizing pure crystalline nickel ferrite nanoparticles. This simple, cost-effective, and environmentally friendly method can be extended to synthesizing other spinel ferrite nanoparticles of interest in nanotechnology.

References

[1] XU Q., WEI Y., LIU Y., JI X., YANG L., GU M., *Solid State Sci.*, 11 (2009), 472.

[2] TIAN M., *Magnetic Material*, Tsinghua University Press, Beijing, 2001.

[3] KHARABE R.G., DEVAN R.S., KANAMADI C.M., CHOUGULE B.K., *J. Alloy. Compd.*, 67 (2008), 463.

[4] KIM W.C., KIM S.J., LEE W.S., KIM C.S., *J. Magn. Magn. Mater.*, 226 (2001), 1418.

[5] SATYANARAYANA L., REDDY K.M., MANORAMA S.V., *Mater. Chem. Phys.*, 82 (2003), 21.

[6] MURDOCK E., SIMMONS R., DAVIDSON R., *IEEE T. Magn.*, 28 (1992), *3078*.

[7] MISHRA S., KARAK N., KUNDU T.K., DAS D., MAITY N., CHKRAVORTY D., *Mater. Lett.*, 60 (2006), 1111.

[8] LI F., WANG H.,WANG L., WANG J., *J. Magn. Magn. Mater.*, 309 (2007), 295.

[9] SUN S., ZENG H., ROBINSON D.B., RAOUX S., RICE P.M., WANG S.X., LI G., *J. Am. Chem. Soc.*, 126 (2004), 2782.

[10] ZHENG Y.Q., TONG Y.C., WANG B., XIE Y., DONG L.H., LD., LIU M.X., *Chinese Sci. Bull.*, 54 (2009), 2998.

[11] HYEON T., CHUNG Y., PARK J., LEE S.S., KIM Y.W., PARK B.H., *J. Phys. Chem. B*, 106 (2002), 683.

[12] GUNJAKAR J.L., MORE A.M., GURAV K.V., LOKHANDE C.D., *Appl. Surf. Sci.*, 254 (2008), 5848.

[13] VLADIKOVA D., YONCHEV H., ILKOV L., KARBANOV S., *J. Magn. Magn. Mat.*, 78 (1989), 420.

[14] VAUTIER R., PAULUS M., *Numerical Data and Functional Relationships in Science and Technology*, Hellwge Ed., Berlin, 1970.

[15] AULOCK VON W.H., *Handbook of Microwave Ferrite*, Section III, Academic Press, New York, 1965.

[16] BOZORTH R.M., *Ferromagnetism*, Van Nostrand D. Co. Inc., 1951.

[17] GORTER E.W., *Philips Res. Rep.*, 9 (1954), 295.

[18] ABRAHAM T., *Am. Ceram. Soc. Bull.*, 73 (1994), 62.

[19] SMIT J., WIJN H.P.J., *Ferrites*, Philips Technical Library, Netherlands, 1959.

[20] GINNAKOPOULOU T., KOMPOTIATIS L., KONTOGEOGAKOS A., KORDAS G., *J. Magn. Magn. Mater.*, 246 (2002), 360.

[21] PATIL D.R., CHOUGULE B.K., *Mater. Chem. Phys.*, 117 (2009), 35.

[22] SHAFI K.V.P.M., GEDANKEN A., PROZOROV R., BALOGH J., *Chem. Mater.*, 10 (1998), 3445.

[23] MUSIC S., POPOVIC S., DALIPI S., *J. Mater. Sci.*, 28 (1993), 1793.

[24] HOCHEPIED J.F., BONVILLE P., PILENI M.P., *J. Phys. Chem.*, 104 (2000), 905.

[25] CROSS W.B., AFFLECK L., KUZNETSOV M.V., *J. Mater. Chem.*, 9 (1999), 2545.

[26] KONISHI Y., KAWAMURA T., ASAI S., *Ind. Eng. Chem. Res.*, 35 (1996), 320.

[27] KIM C., *J. Appl. Phys.*, 85 (1999), 5223.

[28] KIM Y.I., KIM D., LEE C.S., *Physica B*, 337 (2003), 42.

[29] BAYKAL A.L., KASAPOGLU N., KOSEOGLU Y.K., TOPRAK M.S., BAYRAKDAR H., *J. Alloy. Compd.*, 464 (2008), 514.

[30] EBRAHIMI S.A.S., AZADMANJIRI J., *J. Non-Cryst. Solids*, 353 (2007), 802.

[31] YANG W., QI Y., MA Y., LI X., GUO X., GAO J., CHEN M., *Mater. Chem. Phys.*, 36 (2004), 192.

[32] MAAZ K., KARIM S., MUMTAZ A., HASANAIN S.K., LIU J., DUAN J.L., *J. Magn. Magn. Mater.*, 321 (2009), 1838.

[33] SAYER G., YI M., *Ceram. Bull.*, 70 (1991), 1173.

[34] AZADMANJIRI J., SEYYED EBRAHIMI S.A., *Phys. Status Solidi C*, 1 (2004), 3414.

[35] HWANG C.C., TSAI J.S., HUANG T.H., *Mater. Chem. Phys.*, 93 (2005), 330.

[36] MAENSIRI S., MASINGBOON C., BANJONG B., SERAPHIN S., *Scripta Mater.*, 56 (2007), 797.

[37] WALDRON R.D., *Phys. Rev.* 99 (1955), 1727.

[38] PRIYADHARSINI P., PRADEEP A., RAO P.S., CHANDRASEKARAN G., *Mater. Chem. Phys.*, 116 (2009), 207.

[39] TAUC J., GRIGOROVICI R., VANCU A., *Phys. Stat. Sol.*, 15 (1966), 627.

[40] ZHANG L., GUANG J.F., ZHAO F., GONG Z.Z., CHIN, *Physica B*, 20 (2011), 047102.

[41] SANGMANEE M., MAENSIRI S., *Appl. Phys. A-Mater.*, 97 (2009), 167.

[42] MONTEMAYOR S.M., GARCIA-CERDA L.A., TORRES-LUBIAN J.R., FERNANDEZ O.S.R., *J. Sol-Gel Sci. Techn.*, 42 (2007), 181.

[43] BERKOWITZ A.E., LAHUT J.A., JACOBS I.S., LEVINSON L.M., FORESTER D.W., *Phys. Rev. Lett.*, 34 (1975), 594.

[44] BERKOWITZ A.E., LAHUT J.A., VANBUREN C.E., *IEEE T. Magn.*, 16 (1980), 184.

[45] COEY J.M.D., *Phys. Rev. Lett.*, 27 (1971), 1140.